

# F<sub>1</sub>-ATPase Is a Highly Efficient Molecular Motor that Rotates with Discrete 120° Steps

Ryohei Yasuda,\*<sup>¶</sup> Hiroyuki Noji,<sup>†‡</sup>

Kazuhiko Kinoshita, Jr.,\*<sup>¶§</sup>

and Masasuke Yoshida<sup>†‡</sup>

\*Department of Physics

Faculty of Science and Technology

Keio University

Yokohama 223-8522

Japan

<sup>†</sup>Research Laboratory of Resources Utilization

Tokyo Institute of Technology

Yokohama 226-8503

Japan

<sup>‡</sup>CREST (Core Research for Evolutional Science and Technology) "Genetic Programming" Team 13

Teikyo University Biotechnology Research

Center 3F

Nogawa 907, Miyamae-ku

Kawasaki 216-0001

Japan

## Summary

A single molecule of F<sub>1</sub>-ATPase, a portion of ATP synthase, is by itself a rotary motor in which a central  $\gamma$  subunit rotates against a surrounding cylinder made of  $\alpha_3\beta_3$  subunits. Driven by three catalytic  $\beta$ s, each fueled with ATP,  $\gamma$  makes discrete 120° steps, occasionally stepping backward. The work done in each step is constant over a broad range of imposed load and is close to the free energy of hydrolysis of one ATP molecule.

## Introduction

ATP, a major currency of energy in the biological world, is synthesized from ADP and phosphate by extracting energy from the flow of protons across a membrane (Mitchell, 1961). The protein machine catalyzing this energy conversion process is the ATP synthase, which is ubiquitous from bacteria to plants and animals. The ATP synthase is a reversible machine: it can pump protons in the reverse direction by hydrolyzing ATP. The enzyme consists of a membrane-embedded, proton-conducting portion (F<sub>0</sub>) and a protruding portion (F<sub>1</sub>) in which ATP is synthesized or hydrolyzed. Isolated F<sub>1</sub>, composed of  $\alpha_3\beta_3\gamma\delta\epsilon$  subunits, only hydrolyzes ATP and is called F<sub>1</sub>-ATPase. Boyer (Boyer and Kohlbrenner, 1981; Boyer, 1997) has proposed that the reactions in F<sub>0</sub> and F<sub>1</sub> are coupled by a common shaft: the proton flow through F<sub>0</sub> rotates the shaft and causes conformational changes in F<sub>1</sub> that result in ATP synthesis. Conversely, ATP hydrolysis in F<sub>1</sub> causes reverse rotation of the shaft and reverse flow of protons. This rotational catalysis model gained support from a crystal structure (Abrahams et al., 1994) of F<sub>1</sub>: a central  $\gamma$  subunit is surrounded by an

$\alpha_3\beta_3$  cylinder, and three catalytic  $\beta$  subunits bearing (an analog of) ATP, ADP, and none are arranged in a unique order around a pseudo 3-fold axis. Sequential ATP hydrolysis would thus rotate  $\gamma$ , as has since been confirmed by various methods (Duncan et al., 1995; Sabbert et al., 1996; Zhou et al., 1996; Aggeler et al., 1997; Noji et al., 1997; Yasuda et al., 1997). Precisely how the free energy of ATP hydrolysis is converted to the mechanical rotation is yet to be worked out (Junge et al., 1997; Kagawa and Hamamoto, 1997; Kinoshita et al., 1998).

In our previous work (Noji et al., 1997), the rotation of  $\gamma$  was directly visualized under an optical microscope by attaching a fluorescent actin filament to  $\gamma$  (Figure 1). The filament rotated continuously in the direction predicted from the crystal structure. The crystal structure also suggests stepwise rotation with pauses every 120°, but the observed rotation was rather smooth (Noji et al., 1997). Here, we show that at low ATP concentrations, rotation of the  $\gamma$ -attached actin is resolved into discrete 120° steps including occasional back steps. In each step, the F<sub>1</sub> bearing actin does mechanical work (against hydrodynamic friction) averaging  $\sim 90$  pN·nm, almost equivalent to the free energy of ATP hydrolysis. Distribution of dwell times between steps suggests hydrolysis of one ATP per step, implying that the efficiency of F<sub>1</sub> is nearly 100%.

## Results

### Observation of Rotation

To observe the rotation of  $\gamma$  under a microscope, we fixed a subcomplex ( $\alpha_3\beta_3\gamma$ ) of F<sub>1</sub> on a surface-bound bead (0.2  $\mu$ m in diameter) through ten histidines (His tag) linked to the amino terminus of each  $\beta$  (Figure 1). A fluorescently labeled actin filament was attached to  $\gamma$  through streptavidin. When ATP was infused in an observation chamber containing many actin-carrying subcomplexes, up to a few percent of the fluorescent actin filaments rotated continuously, invariably counterclockwise when viewed from above in Figure 1. Others only fluctuated, in rare cases up to a few accumulated turns in either direction, or were immobile, as previously reported (Noji et al., 1997). Nonrotating filaments were probably obstructed by nearby proteins or other beads, or by the glass surface against which oblique filaments would be pressed. Also, some of the subcomplexes on the bead might have been inactive. Below we focus on fully active and unobstructed  $\alpha_3\beta_3\gamma$  subcomplexes that rotated an actin filament at least five continuous revolutions in a regular (though stochastic) fashion without a noticeably unnatural intermission.

### Load Dependence of the Rotational Rate

The hydrodynamic friction against an actin filament rotating around one end is essentially proportional to the cube of its length,  $L$ ; the rotational frictional drag coefficient  $\xi$  is given by (Hunt et al., 1994)  $\xi = (4\pi/3)\eta L^3/[\ln(L/2r) - 0.447]$ , where  $\eta$  ( $10^{-3}$  N·m·s<sup>-2</sup>) is the viscosity of the medium and  $r$  (5 nm) the radius of the filament. Thus, the rotation

<sup>§</sup>To whom correspondence should be addressed.

<sup>¶</sup>These authors contributed equally to this work.

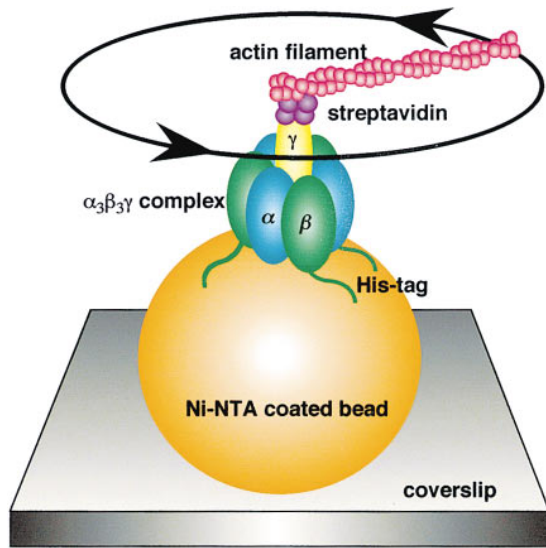


Figure 1. Experimental System (Not to Scale)

was slower for longer actin filaments (Figure 2a). At 2 mM (and 20  $\mu$ M) ATP, the rotational rates were consistent with a constant frictional torque (the drag coefficient  $\times$  the rotational rate) of  $\sim 40$  pN-nm (red line in Figure 2a), indicating that the subcomplex produced this much of torque irrespective of the frictional load. This torque times  $2\pi/3$ ,  $\sim 80$  pN-nm, is the work done in one-third of a revolution. On the other hand, the free energy of

hydrolysis of one ATP,  $\Delta G_{ATP}$ , is  $\sim 80$  pN-nm under physiological conditions (Stryer, 1995). Thus, if one ATP is hydrolyzed per  $120^\circ$  revolution as implicated in the Boyer's rotational catalysis model (Boyer and Kohlbrenner, 1981; Boyer, 1997), the efficiency of the  $\alpha_3\beta_3\gamma$  subcomplex is  $\sim 100\%$ .

$\Delta G_{ATP}$  in our samples was not well defined, because the medium contained an ATP-regenerating system. We therefore measured the rotational rate in the presence of 2 mM ATP, 10  $\mu$ M ADP, and 0.1 or 10 mM phosphate (pH 7.0), where  $\Delta G_{ATP}$  would be 110 or 90 pN-nm, respectively (Stryer, 1995). Within experimental scatter, the rotational rates were indistinguishable from those with the ATP-regenerating system (Figure 2a), assuring  $\sim 100\%$  efficiency for the one-ATP/ $120^\circ$  scenario.

The scatter in experimental points in Figure 2a does not allow precise estimation of the efficiency; if true rotational rates are half those given by the red line in Figure 2a, the torque would be as low as 20 pN-nm (efficiency  $\sim 50\%$ ). However, we think that points giving higher rotational rates are more reliable, because any obstructions or impeding factors such as the higher-than-bulk friction near the glass surface (Hunt et al., 1994) would reduce the rate, whereas gross statistical overestimate is unlikely for the rate determined as an average over at least five revolutions.

#### ATP Dependence

The rotational rate decreased at ATP concentrations below  $\sim 2$   $\mu$ M (Figure 2a). For short filaments (0.8–1.2

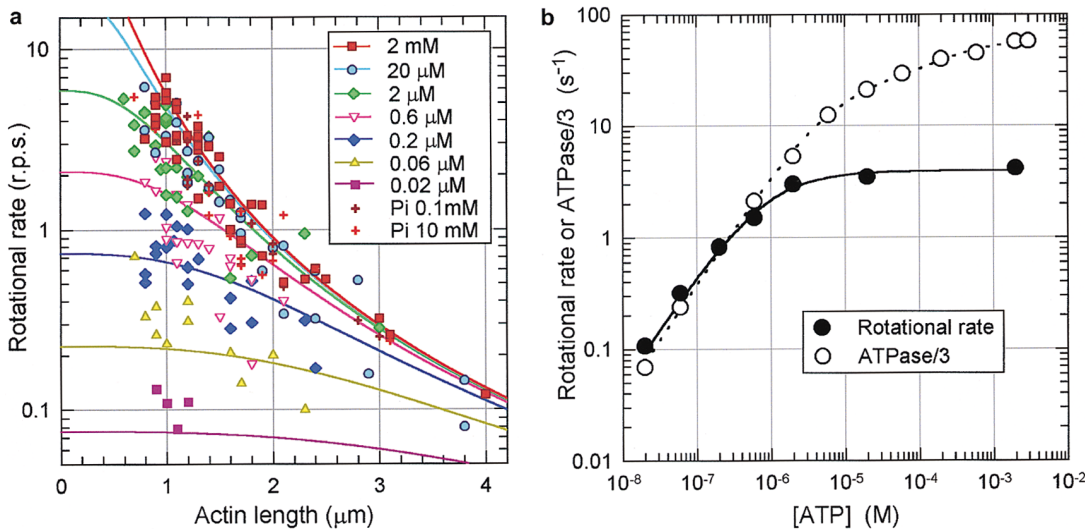


Figure 2. Load and ATP Dependence of the Rotational Rate

(a) Rotational rate in revolutions per second (r.p.s.), averaged over  $>5$  revolutions, versus the length of the actin filament at indicated ATP concentrations. + (dark red) at 2 mM ATP, 10  $\mu$ M ADP, and 0.1 mM phosphate in the absence of ATP regenerating system (see Experimental Procedures); + (red), the same except phosphate was 10 mM; in all others except for some points for 2 mM ATP, the medium contained the ATP regenerating system. Rotation was observed with the intensified CCD camera at a resolution of 33 ms. Filaments that rotated around one end for  $>5$  revolutions without an unnatural intermission were analyzed. At 20 and 60 nM ATP, the rotation was stepwise even at the low temporal resolution; those filaments for which the angular distribution showed a single high peak ( $>10$  times higher than other peaks) were judged obstructed and not scored. Red line shows the rotational rate,  $\omega/2\pi$ , where  $\omega$  is the angular velocity, under a constant torque,  $N$ , of 40 pN-nm:  $\omega = N/\xi$ , where  $\xi$  is the drag coefficient defined in text. Other lines show  $1/(3\tau_{120^\circ})$  explained in text.

(b) Rotational rate  $v$  of short (0.8–1.2  $\mu$ m) filaments (filled circles), and solution ATPase rate  $V$  divided by three (open circles). Solid line shows  $v = v_{max}[ATP]/([ATP] + K_m^{rot})$ , where  $v_{max} = 3.9$  r.p.s and  $K_m^{rot} = 0.8$   $\mu$ M; dashed line shows  $V = (k_{cat}^1 K_m^{ATP} [ATP] + k_{cat}^2 [ATP]^2)/([ATP]^2 + K_m^{ATP,2} [ATP] + K_m^{ATP,1} K_m^{ATP,2})$ , where  $k_{cat}^1 = 75$   $s^{-1}$ ,  $k_{cat}^2 = 177$   $s^{-1}$ ,  $K_m^{ATP,1} = 6.6$   $\mu$ M, and  $K_m^{ATP,2} = 285$   $\mu$ M. The ATPase rate was determined between 3–13 s after addition of the enzyme; the rate gradually decreased with time to a steady level several times lower than the initial value (the so-called MgADP inhibition) (Jault et al., 1995; Matsui et al., 1997).

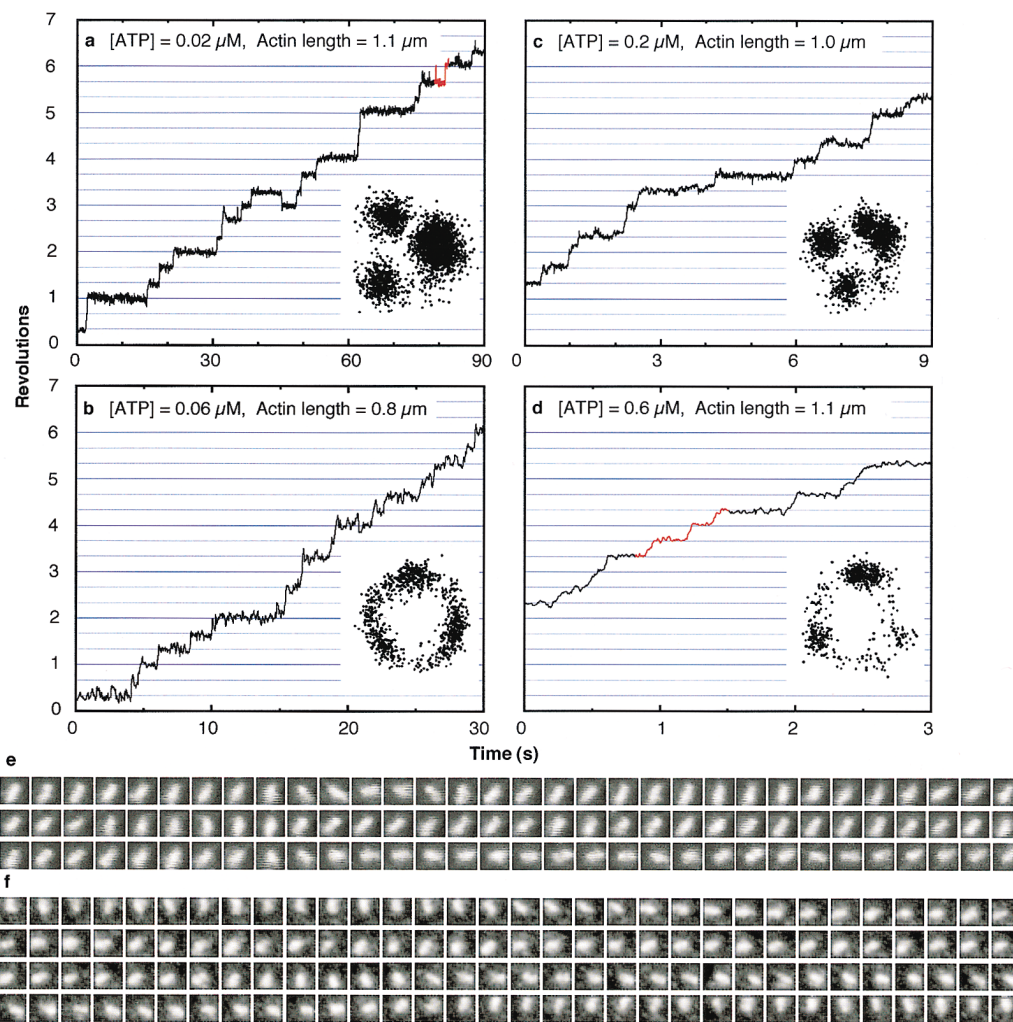


Figure 3. Stepwise Rotation at Low ATP Concentrations

Insets show the trace of the centroid of the actin image. Images of the actin filaments in (a) and (d) (colored regions) are shown in (e) (33 ms intervals) and (f) (5 ms intervals), respectively. (a) and (b) were recorded with the intensified CCD camera, and (c) and (d) with the fast-scan cooled CCD camera.

μm), the rates at 0.02–2000 μM ATP were fitted with a simple Michaelis-Menten kinetics (solid line in Figure 2b), suggesting that ATP binding was rate limiting at submicromolar ATP and that, at least in this range, the rotation was fueled with individual ATP molecules without requiring simultaneous consumption of two or more ATPs (but see below).

The rate of ATP hydrolysis by the  $\alpha_3\beta_3\gamma$  subcomplex without actin was measured in solution (Figure 2b, open circles). At low ATP concentrations, the unloaded ATPase rate divided by three roughly coincided with the rotational rate, in accord with the contentions that one ATP is consumed per 120° and that ATP binding is rate limiting at low ATP. (The ATPase rate was slightly lower than the rotational rate, presumably because some of the subcomplexes in the solution were in the MgADP-inhibited form [Jault et al., 1995; Matsui et al., 1997]; in the rotation assay, those inactive ones were ignored.) At higher ATP concentrations, the rotational rate was saturated at the level determined by the frictional load (see below), whereas the unloaded ATPase showed an

ATP dependence characteristic of F<sub>1</sub> from various sources (Gresser et al., 1982; Grubmeyer et al., 1982; Kato et al., 1995; Muneyuki et al., 1997). If the rotation and ATP hydrolysis are tightly coupled, the rate of ATP hydrolysis on the actin-carrying subcomplex will parallel the rotational rate (filled circles in Figure 2b). We have been unable to measure reliably the ATPase rate under loaded conditions (and the ATPase activity of the surface immobilized enzyme).

Generally, the rotational rate will depend on both the frictional load and ATP binding. One of the simplest schemes would be one in which the cycle time for unloaded ATPase,  $\tau_{ATP}$ , is prolonged by an amount,  $\tau_{step}$ , with which the actin filament travels 120° against friction: the time per 120° revolution,  $\tau_{120^\circ}$ , equals  $\tau_{ATP} + \tau_{step}$ . If the subcomplex produces a torque,  $N$ , to drive the actin filament,  $\tau_{step}$  equals  $(2\pi/3)\xi/N$ , where  $\xi$  is the drag coefficient. Lines in Figure 2a show the calculated rotational rate,  $1/(3\tau_{120^\circ})$ , for  $\tau_{ATP}$  calculated from the dashed line in Figure 2b and a constant torque,  $N$ , of 40 pN·nm. The simple scheme explains the data fairly well. At least for

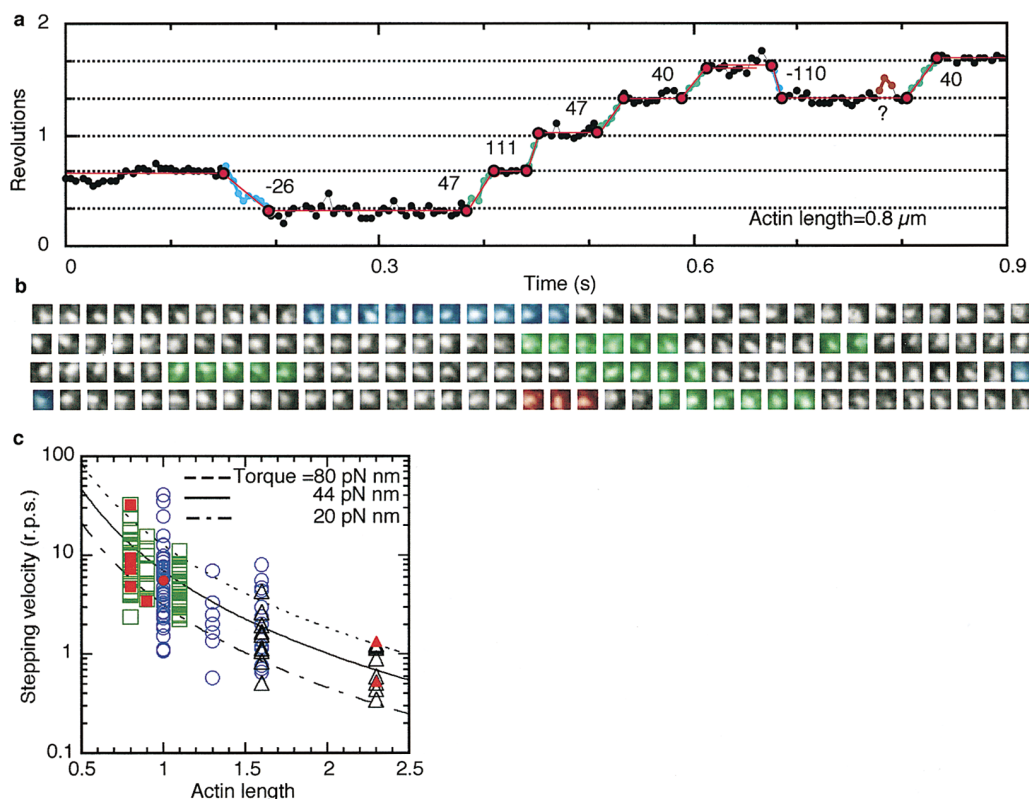


Figure 4. Driving Torque for the Steps

(a) Estimation of the stepping velocity. The revolution versus time data in the vicinity of a step identified by eye are fitted with linear segments, horizontal ones for pauses, and an oblique one for the step (red circles show the intersections between segments). The torque in each step was calculated as  $\omega\xi$ ,  $\omega$  being the angular velocity, and shown as a number in units of pN-nm.

(b) Corresponding filament images at 5 ms intervals. The center of each image frame is the center of rotation; note the position of the filament rather than its orientation, which is difficult to discern in these images. Steps are shown in the same colors as in (a).

(c) Distribution of stepping velocities as estimated in (a). Black triangles, [ATP] = 60 nM; blue circles, 200 nM; green squares, 600 nM. Red symbols show back steps. Lines indicate velocities expected for indicated torque values. The torque averaged over all steps was 44 pN-nm.

the filament length  $\geq 1 \mu\text{m}$  and ATP concentrations between 20 nM and 2 mM, the subcomplex appears to produce a constant torque of  $\sim 40$  pN-nm or a constant work per  $120^\circ$  of  $\sim 80$  pN-nm.

### Steps

In the crystal (Abrahams et al., 1994), three  $\beta$  subunits bearing (an analog of) ATP, ADP, and none are arranged clockwise when viewed from the top in Figure 1. If hydrolysis were to proceed in the crystal, the next order would be ADP, none, and ATP. Thus, the central  $\gamma$  would turn counterclockwise, as was actually observed (Noji et al., 1997; Kinosita et al., 1998). The fact that the asymmetric arrangement is stable in the crystal also predicts that the rotation of  $\gamma$  would be stepwise, pausing every  $120^\circ$  at the stable structure. Indeed, the actin filament showed clear  $120^\circ$  steps at submicromolar ATP (Figure 3). Not all samples gave regular steps; often the average dwell times at the three positions were not equal (Figure 3, insets), and in some filaments pauses at a fourth position were also observed. These irregularities are probably due to surface obstructions. In no cases did we observe pauses at six regular positions that would indicate transient association of  $\gamma$  with  $\alpha$ .

Actin movement during each step was resolved at 5 ms resolution. The stepping time,  $\tau_{\text{step}}$ , was determined as shown in Figure 4a. In Figure 4c, the stepping velocity in revolutions per second,  $1/(3\tau_{\text{step}})$ , is plotted against the actin length. Although the variation in the velocities for individual steps is very large (in part due to poor experimental precision), the data indicate that the steps were made at an average torque of 44 pN-nm irrespective of the frictional load (solid line in Figure 4c), as was also the case for the average velocity at high ATP concentrations (Figure 2a). The average work done in a step is  $\sim 90$  pN-nm. Whether steps are contiguous (at high ATP concentrations) or discrete,  $F_1$  (the subcomplex) puts a free-energy equivalent of one ATP into each step.

Figure 5 shows histograms of dwell times between successive steps. If each dwell is terminated by binding of one ATP, the histogram should be exponential. In contrast, termination by two or more ATPs would produce an upward convex histogram passing through the origin (red and green lines; see below), because short dwells would be scarce in these cases (Higuchi et al., 1997; Hua et al., 1997). The data at 20 and 60 nM ATP are basically exponential (black lines), suggesting one

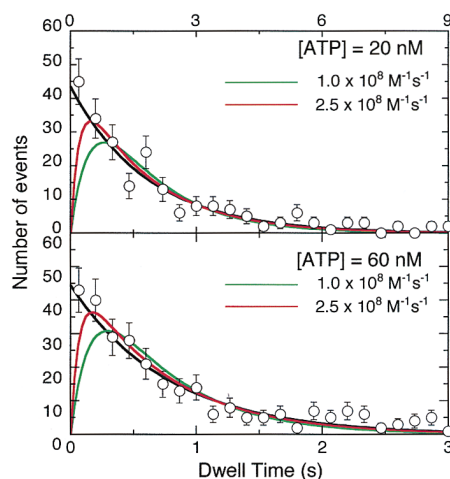


Figure 5. Histograms of Dwell Times between Steps

Error bars show the square root of the count, which is the expected standard deviation. Black lines indicate exponential fits:  $\text{const.} \times \exp(-k_{\text{on}}[\text{ATP}]t)$ , where  $k_{\text{on}}$  is the rate constant for ATP binding ( $2.7 \times 10^7 \text{ M}^{-1}\text{s}^{-1}$  at 20 nM ATP and  $2.2 \times 10^7 \text{ M}^{-1}\text{s}^{-1}$  at 60 nM) and  $t$  is the dwell time. Green and red lines show fits with two exponentials (simultaneous consumption of rapidly and slowly bound ATP) (Higuchi et al., 1997; Hua et al., 1997):  $\text{const.} \times \{\exp(-k_{\text{on}}^{\text{slow}}[\text{ATP}]t) - \exp(-k_{\text{on}}^{\text{rapid}}[\text{ATP}]t)\}$ , where  $k_{\text{on}}^{\text{rapid}}$  was fixed at the indicated values. The sum of residuals,  $\chi^2 = \sum w(n_{\text{obs}} - n_{\text{calc}})^2$ , where  $n$  is the number of events and  $w = 1/n_{\text{obs}}$  for  $n_{\text{obs}} > 0$  and  $w = 1$  for  $n_{\text{obs}} = 0$ , was 29, 39, and 58 for the black, red, and green lines for 20 nM ATP, and 33, 40, and 61 for 60 nM ATP, respectively. For the data at 20 nM ATP, dwell times up to 60 s were analyzed, of which 217 were shorter than 9 s and 10 were between 9 s and 30 s; dwell times longer than 30 s were absent except for extremely long ones that forced the observation to a termination. For the data at 60 nM ATP, dwell times up to 18 s were analyzed, of which 274 were below 3 s and 15 were between 3 s and 18 s; longer dwells led to a termination of observation.

ATP per step; the slight deviation at long dwell times presumably resulted from surface obstructions. The exponential fit gives the rate constant for ATP binding ( $k_{\text{on}}$ ) of  $2.7 \times 10^7$  (20 nM ATP) and  $2.2 \times 10^7$  (60 nM)  $\text{M}^{-1}\text{s}^{-1}$ , which agree with each other within experimental precision. These values are consistent with literature values (Gresser et al., 1982; Grubmeyer et al., 1982; Cunningham and Cross, 1988) of the order of  $10^7 \text{ M}^{-1}\text{s}^{-1}$  for F<sub>1</sub>-ATPase of various origins at submicromolar to micromolar ATP. The values are somewhat greater than the rate constant of  $1.5 \times 10^7 \text{ M}^{-1}\text{s}^{-1}$  estimated from the average rotational rate in Figure 2b, because the abundance of long dwells (presumably an artifact due to surface obstructions) has a smaller effect in the exponential analysis (black lines).

Backward steps were observed occasionally (Figures 3 and 4). Interestingly, the back steps were as fast as forward steps, implying that the back steps also required an energy of  $\sim$ one ATP, or 20 times the average thermal energy (Figure 4c, red symbols). A likely explanation, among others (see below), is that each back step also consumes one ATP. Clear back steps have also been observed with a linear motor kinesin (Coppin et al., 1997), but the kinesin was pulled backward with optical tweezers and thus those back steps did not require supply of energy from ATP.

## Discussion

### Rotational Catalysis

The three catalytic sites of F<sub>1</sub>-ATPase show negative cooperativity for substrate binding and positive cooperativity for catalysis (Boyer, 1997). The basic scheme, though not yet settled, is as follows. Binding of the first ATP to an empty F<sub>1</sub> is quite tight, characterized by a dissociation constant of  $\sim$ pM (Grubmeyer et al., 1982; Soud and Penefsky, 1995) or  $\sim$ nM (Xiao and Penefsky, 1994). The overall catalysis when only one of the three catalytic sites is occupied (unisite catalysis) is slow. Binding of a second ATP greatly promotes the release of the first hydrolysis products (Cunningham and Cross, 1988; Milgrom et al., 1998). The apparent Michaelis-Menten constant ( $K_m$ ) for this process is in the  $\mu\text{M}$  range. Below this  $K_m$ , the average occupancy of the catalytic sites is slightly more than one (bisite catalysis). Trisite catalysis may also occur at high ATP concentrations. The apparent  $K_m$ s for the three modes (unisite, bisite, and trisite) vary considerably among different samples. At submicromolar ATP, however, the bisite regime appears to be the norm in all systems. Thus, our data (Figures 2 and 3) show that bisite catalysis, and trisite if it occurs, accompanies rotation of  $\gamma$ . In the bisite and putative trisite regimes, hydrolysis of ATP in ATP synthase (F<sub>o</sub>F<sub>1</sub>) is coupled to proton pumping (Muneyuki and Hirata, 1988; Muneyuki et al., 1989), presumably through the rotation of  $\gamma$  as suggested (Boyer, 1997).

In bisite catalysis, the second ATP will bind to one of the two empty sites. The correct choice that assures counterclockwise rotation will most probably be dictated by the central, asymmetric  $\gamma$ , which would force the two empty  $\beta$ s into different conformations with different affinities for ATP. Alternatively, the affinities of the two could be similar, but the rotation of  $\gamma$  might be somehow inhibited when ATP binds to the wrong site. The back steps we observed under the presumed bisite condition (Figures 3 and 4) likely resulted from binding of ATP to the wrong site. If so, the implications are (i) the affinity of the wrong site for ATP is not too low compared to the affinity of the correct site, and (ii) backward rotation can occur when two catalytic sites carrying ATP and its hydrolysis product(s) are arranged in the wrong order. Point (ii) further implicates that it is primarily the  $\beta$  carrying ATP that determines the orientation of  $\gamma$ . As to point (i), we occasionally observed rapid succession of forward and back steps (e.g., the red part in Figure 3a), suggesting a possibility that the affinity for the wrong site might be transiently high after a forward step.

The high and constant mechanical output of the F<sub>1</sub> motor imposes restrictions on possible mechanisms. In principle,  $\gamma$  could make a 120° step if the surrounding  $\alpha_3\beta_3$  cylinder, in response to changes of the bound nucleotides, adopts a next conformation that energetically favors a new orientation of  $\gamma$  advanced by 120°;  $\gamma$  could jump into the new orientation by thermal activation. This scheme does not require a metastable intermediate conformation(s). When an actin filament is attached, however, the jump has to produce mechanical work of  $\sim$ 20 times the thermal energy in addition to overcoming an inherent activation barrier. Such a jump would be too

infrequent to account for the observed rotation (Kinosita et al., 1998; also see below). A possible way out is that the potential well in the next conformation of the  $\alpha_3\beta_3$  cylinder is downhill for a large part of the path connecting the current orientation of  $\gamma$  to one  $120^\circ$  ahead (i.e., the cylinder is made to pull [and/or push]  $\gamma$  all the way to the next orientation). Otherwise, the jump has to be made in small substeps, each expending energy supplied by a change(s) in bound nucleotides (e.g., phosphate release). Substeps were not seen in our records at the limited time resolution.

The constant mechanical output independent of the actin length could be explained if a "spring" exists between the actin filament and  $\gamma$ , and/or between the  $\alpha_3\beta_3$  cylinder and glass surface;  $\gamma$  rotates first to the next position in the cylinder, and then the spring pulls the actin filament. For this, however, the spring(s) has to be of the right strength such that the potential energy stored by the rotation of  $\gamma$  is  $\sim \Delta G_{ATP}$ .  $\gamma$  would not be able to wind up a stronger spring, whereas a weaker spring would not pull the filament as fast as actually observed. (A weak spring could be wound beyond  $120^\circ$  to deliver a strong torque, but then the actin filament would rotate past  $120^\circ$  without pausing.) A more likely scenario, if a spring operates, is that an effective spring (downhill potential) is introduced between the  $\alpha_3\beta_3$  cylinder and  $\gamma$  when the cylinder adopts the next conformation and is ready to pull  $\gamma$ . The built-in spring may well be designed to produce work close to  $\Delta G_{ATP}$ .

### Back Steps

As shown in Figure 4c, the back steps are as fast as the forward steps, characterized by short stepping times,  $\tau_{120^\circ}$ , that would require a constant work per step,  $W$ , as large as  $\sim 90$  pN·nm ( $\tau_{120^\circ} = (2\pi/3)^2\xi/W$ ). Because the work,  $W$ , amounts to 20 times the thermal energy, the steps, at least most of the forward ones, should be powered by ATP. However, the back steps are relatively scarce (several percent of all steps at 60–600 nM ATP or once in 100–10 s), raising the possibility that they might result from thermal fluctuations. Below we discuss whether thermal motion can in fact account for the rapid back steps.

First, consider the possibility that a "clutch" between  $\gamma$  and the  $\alpha_3\beta_3$  cylinder, or between  $\gamma$  and actin, is occasionally disengaged and allows free rotational diffusion of the actin filament. The rotational diffusion constant,  $D$ , for the actin filament is given by  $D = k_B T/\xi$ , where  $k_B T$  is the average thermal energy ( $\sim 4.1$  pN·nm). On the average, rotational diffusion over  $120^\circ$  takes a time  $\sim (2\pi/3)^2/2D$ , which is longer than the  $\tau_{120^\circ}$  above by a factor of  $W/2k_B T \sim 10$ . Occasionally, however, the filament rotates beyond  $120^\circ$  over the time interval of  $\tau_{120^\circ}$ . This probability is given, for  $W \gg k_B T$ , by  $(k_B T/\pi W)^{1/2} \exp(-W/4k_B T)$ , which is  $\sim 0.0005$  for  $W = 90$  pN·nm (twice this value if the filament is locked at the  $120^\circ$  position upon the first arrival). That is, free rotational diffusion can carry an actin filament with an effective velocity of ( $\geq$ )  $120^\circ$  per  $\tau_{120^\circ}$  at a frequency of once in  $\sim 2000\tau_{120^\circ}$ . For a  $1 \mu\text{m}$  filament for which  $\tau_{120^\circ}$  is  $\sim 0.05$  s, the rapid diffusional excursion occurs once in  $\sim 100$  s, which is not too infrequent compared to the observed back steps. However,

the presence of clear pauses between steps (Figures 3 and 4) implies that the clutch must be engaged for most of the time, suggesting that rapid back steps by free diffusion should be less frequent. Moreover, most of diffusional excursions over  $120^\circ$  should be much slower, contradicting the high average velocity for the observed steps (Figure 4c). It seems difficult to account for the observed back steps by purely diffusive processes.

If thermal diffusion is assisted by a potential slope, an actin filament could rotate rapidly. Suppose that the potential for backward rotation is of a sawtooth type, starting with a steep uphill followed by a downhill toward a position  $120^\circ$  behind. If the slope for the downhill portion is  $\sim W$  per  $120^\circ$ , a back step with the correct velocity is expected. However, the passage through the uphill portion, with a height at least  $W$ , is a rare event. If the width of the uphill portion is  $\Delta\theta$ , the frequency will be in the order of once in  $(\Delta\theta^2/2D)\exp(W/k_B T)$ , which, for a  $1 \mu\text{m}$  filament, is  $10^5$  s for  $\Delta\theta$  as small as  $1^\circ$ .

Different types of potential and/or minor pathways of ATP hydrolysis may account for the back steps without requiring a complete cycle of ATP hydrolysis. We think, however, that ATP binding to the wrong site is the most simple and plausible explanation for the observed back steps.

### Thermodynamic Efficiency

Our rotation assay indicates that each  $120^\circ$  step requires hydrolysis of one ATP. Strictly, however, the data do not rule out the consumption of two ATPs per step. If the first ATP always binds rapidly and if binding of the second ATP always results in simultaneous release of two ADPs, the average rotational rate would still be proportional to the ATP concentration, and the histogram of dwell times between steps would be apparently exponential. For this to be the case, the rate constant for the first ATP binding should be  $>10^8 \text{ M}^{-1}\text{s}^{-1}$ , because otherwise the histogram of dwell times will significantly deviate from exponential near the origin (Figure 5, green and red lines). A binding rate  $>\sim 10^8 \text{ M}^{-1}\text{s}^{-1}$  has not been reported for either unisite or bisite catalysis. Thus, simultaneous consumption of two ATPs is unlikely, and each step is most probably made at  $\sim 100\%$  efficiency. The high efficiency accords with the fully reversible nature of this motor. A model for  $F_1$ -ATPase has predicted such a high efficiency (Oosawa and Hayashi, 1986).

Consumption of ATP without rotation is not noticed in our rotation assay. If such decoupling occurs frequently, the thermodynamic efficiency (mechanical work divided by the free energy of all ATPs hydrolyzed) would be much lower than 100%. An argument against this possibility is the agreement between the rotational rate and ATPase rate (Figure 2b), but the rate of ATP hydrolysis may have been underestimated, due to the MgADP inhibition (Jault et al., 1995), by an unknown amount. In the case of myosin motor, which is loosely coupled, its mechanical output as well as the thermodynamic efficiency vary greatly depending on the load (Huxley, 1957).  $F_1$ , in contrast, outputs a constant energy over a wide range of load (Figures 2 and 4), suggesting tight rather than loose coupling. Another reversible motor, the bacterial flagellar motor, which is driven by proton

flow, has been claimed to be tightly coupled and to operate at 100% efficiency at high load (Meister et al., 1987), although a loose coupling scenario has also been advocated (Oosawa and Hayashi, 1986). A definite conclusion on F<sub>1</sub> awaits measurement of hydrolysis on rotating F<sub>1</sub> with single fluorophore imaging (Funatsu et al., 1995; Sase et al., 1995, 1997).

#### Experimental Procedures

##### Proteins

A mutant ( $\alpha$ -C193S,  $\gamma$ -S107C)  $\alpha_3\beta_3\gamma$  subcomplex derived from a thermophilic *Bacillus* PS3 was biotinylated at the sole cysteine ( $\gamma$ -107) and conjugated with streptavidin (Noji et al., 1997). The ATPase activity in solution was estimated from the oxidation of NADH coupled to the ATPase reaction (Kato et al., 1995). Rabbit skeletal actin filaments were biotinylated and stained with phalloidin-tetramethylrhodamine B isothiocyanate conjugate as in our previous report (Noji et al., 1997) but without cross-linking. Labeled actin was centrifuged twice in solution A (50 mM KCl, 2 mM MgCl<sub>2</sub>, 10 mM MOPS-KOH [pH 7.0]) to remove free dye and nucleotides. The sum of free ATP and ADP in 370 nM actin was estimated by luciferin-luciferase assay (Deluca and McElroy, 1978), after conversion of ADP to ATP by incubation with 0.2 mg/ml creatine kinase and 2.5 mM creatine phosphate for 30 min at room temperature, to be  $\approx$ <50 nM and did not increase for at least several weeks.

##### Ni-NTA Beads

To 1% (w/v) suspension of amino polystyrene beads (0.224  $\mu$ m diameter, Polysciences) in 100 mM MOPS-KOH (pH 7.0), 10 mM ethylene glycolbis-[succinimidylsuccinate] was added and incubated for 15 min at room temperature. Then, 100 mM AB-NTA (*N*-[ $\alpha$ -carboxypentyl]-iminodiacetic acid, Dojindo) was added and incubated for 60 min. The beads were washed four times with 100 mM MOPS-KOH and four times with 10 mM NiCl<sub>2</sub> plus 10 mM glycine. Unbound Ni<sup>2+</sup> was removed by washing four times with 100 mM MOPS-KOH.

##### Rotation Assay

A flow chamber was constructed of two coverslips (bottom, 24  $\times$  36 mm<sup>2</sup>; top, 18  $\times$  18 mm<sup>2</sup>) separated by 50  $\mu$ m spacers (Noji et al., 1997). One chamber volume ( $\sim$ 10  $\mu$ l) of 0.1 % Ni-NTA beads in solution A plus 2 mM (total 4 mM) MgCl<sub>2</sub> was infused into the flow chamber and allowed to adhere to the glass surface for 15 min, resulting in a bead density of several beads per 5  $\times$  5  $\mu$ m<sup>2</sup>. The chamber was washed twice with 3 vol of solution B (solution A plus 10 mg/ml BSA). Infusion, incubation, and washing were repeated as follows: 10 nM streptavidin- $\alpha_3\beta_3\gamma$  in solution B (1 vol); 2 min incubation; washing twice with solution B (3 vol); infusion of 37 nM labeled actin filaments (1.5 vol); 15 min incubation; washing with solution B (3 vol); infusion of 2 vol of solution C (solution B plus 0.5% 2-mercaptoethanol, 0.2 mg/ml glucose oxidase, 30 U/ml catalase, 6 mg/ml glucose, and an ATP regenerating system consisting of 0.2 mg/ml creatine kinase and 2.5 mM creatine phosphate; ATP + ADP contamination in this solution,  $\approx$ <5 nM) containing a desired amount of MgATP (2 mM excess MgCl<sub>2</sub>). The chamber was observed on an inverted fluorescence microscope (TMD 300, Nikon) at 22–24°C. Actin rotation could be observed for 30–40 min. Washing with 500 mM imidazole in solution D (solution A plus 5 mg/ml BSA) removed  $\sim$ 80% of actin filaments, whereas 500 mM KCl in solution D removed only  $\sim$ 20%. Without Ni-NTA beads or with amino beads without Ni-NTA, no actin filaments were bound on the glass surface. These results ensure that the actin filaments were attached to the subcomplexes which were attached to the beads through histidine tags.

##### Image Analysis

Fluorescence images were recorded with an intensified (KS-1381, Videoscope) CCD camera (Dage MTI) on an 8 mm video tape. Rapid recording was made with a fast-scan cooled CCD camera (ARGUS/HiSCA, Hamamatsu Photonics) at 190 frames per second. Filaments with the rotation axis at one end were selected, and the centroid

of the filament image was calculated on an image processor (DIPS-C2000, Hamamatsu Photonics) (Noji et al., 1997). From the circular movement of the centroid (Figure 3, insets), rotation angles were calculated.

#### Acknowledgments

We thank Yoshie Harada, Hiroyasu Itoh, Toru Hisabori, Eiro Mune-yuki, Toyoki Amano, and Shin'ichi Ishiwata for critically reading the manuscript; Tadashi Matsui for constructing subcomplex expression system; Shin'ichi Ishiwata for the fast camera; and Makoto Hosoda (Hamamatsu Photonics) for image processing. This work was supported in part by Grants-in-Aid from Ministry of Education, Science, Sports and Culture of Japan (K. K., M. Y.) and a Keio University Special Grant-in-Aid (K. K.). R. Y. is a Research Fellow of the Japan Society for the Promotion of Science.

Received April 14, 1998; revised May 11, 1998.

#### References

- Abrahams, J.P., Leslie, A.G.W., Lutter, R., and Walker, J.E. (1994). Structure at 2.8 Å of F<sub>1</sub>-ATPase from bovine heart mitochondria. *Nature* 370, 621–628.
- Aggeler, B., Ogilvie, I., and Capaldi, R.A. (1997). Rotation of a  $\gamma$ -e subunit domain in the *Escherichia coli* F<sub>1</sub>F<sub>0</sub>-ATP synthase complex. *J. Biol. Chem.* 272, 19621–19624.
- Boyer, P.D. (1997). The ATP synthase: a splendid molecular machine. *Annu. Rev. Biochem.* 66, 717–749.
- Boyer, P.D., and Kohlbrenner, W.E. (1981). The present status of the binding-change mechanism and its relation to ATP formation by chloroplasts. In *Energy Coupling in Photosynthesis*, B.R. Selman and S. Selman-Reimer, eds. (Amsterdam: Elsevier), pp. 231–240.
- Coppin, C.M., Pierce, D.W., Hsu, L., and Vale, R.D. (1997). The load dependence of kinesin's mechanical cycle. *Proc. Natl. Acad. Sci. USA* 94, 8539–8544.
- Cunningham, D., and Cross, R.L. (1988). Catalytic site occupancy during ATP hydrolysis by MF<sub>1</sub>-ATPase. *J. Biol. Chem.* 263, 18850–18856.
- Deluca, M., and McElroy, W.D. (1978). Purification and properties of firefly luciferase. *Methods Enzymol.* 57, 3–15.
- Duncan, T.M., Bulygin, V.V., Zhou, Y., Hutcheon, M.L., and Cross, R.L. (1995). Rotation of subunits during catalysis by *Escherichia coli* F<sub>1</sub>-ATPase. *Proc. Natl. Acad. Sci. USA* 92, 10964–10968.
- Funatsu, T., Harada, Y., Tokunaga, M., Saito, K., and Yanagida, T. (1995). Imaging of single fluorescent molecules and individual ATP turnovers by single myosin molecules in aqueous solution. *Nature* 374, 555–559.
- Gresser, M.J., Myers, J.A., and Boyer, P.D. (1982). Catalytic site cooperativity of beef heart mitochondrial F<sub>1</sub> adenosine triphosphatase. *J. Biol. Chem.* 257, 12030–12038.
- Grubmeyer, C., Cross, R.L., and Penefsky, H.S. (1982). Mechanism of ATP hydrolysis by beef heart mitochondrial ATPase. *J. Biol. Chem.* 257, 12092–12100.
- Higuchi, H., Muto, E., Inoue, Y., and Yanagida, T. (1997). Kinetics of force generation by single kinesin molecules activated by laser photolysis of caged ATP. *Proc. Natl. Acad. Sci. USA* 94, 4395–4400.
- Hua, W., Young, E.C., Fleming, M.L., and Gelles, J. (1997). Coupling of kinesin steps to ATP hydrolysis. *Nature* 388, 390–393.
- Hunt, A.J., Gittes, F., and Howard, J. (1994). The force exerted by a single kinesin molecule against a viscous load. *Biophys. J.* 67, 766–781.
- Huxley, A.F. (1957). Muscle structure and theories of contraction. *Prog. Biophys. Mol. Biol.* 7, 255–318.
- Jault, J.-M., Matsui, T., Jault, F.M., Kaibara, C., Mune-yuki, E., Yoshida, M., Kagawa, Y., and Allison, W.S. (1995). The  $\alpha_3\beta_3\gamma$  complex of the F<sub>1</sub>-ATPase from the thermophilic *Bacillus* PS3 containing the  $\alpha$ -D261N substitution fails to dissociate inhibitory Mg ADP from a catalytic site when ATP binds to noncatalytic sites. *Biochemistry* 34, 16412–16418.

- Junge, W., Lill, H., and Engelbrecht, S. (1997). ATP synthase: an electrochemical transducer with rotatory mechanics. *Trends Biochem. Sci.* *22*, 420–423.
- Kagawa, Y., and Hamamoto, T. (1997). Intramolecular rotation in ATP synthase: dynamic and crystallographic studies on thermophilic  $F_1$ . *Biochem. Biophys. Res. Commun.* *240*, 247–256.
- Kato, Y., Sasayama, T., Muneyuki, E., and Yoshida, M. (1995). Analysis of time-dependent change of *Escherichia coli*  $F_1$ -ATPase activity and its relationship with apparent negative cooperativity. *Biochim. Biophys. Acta* *1231*, 275–281.
- Kinosita, K., Jr., Yasuda, R., Noji, H., Ishiwata, S., and Yoshida, M. (1998).  $F_1$ -ATPase: a rotary motor made of a single molecule. *Cell* *93*, 21–24.
- Matsui, T., Muneyuki, E., Honda, M., Allison, W.S., Dou, C., and Yoshida, M. (1997). Catalytic activity of the  $\alpha_3\beta_3\gamma$  complex of  $F_1$ -ATPase without noncatalytic nucleotide binding site. *J. Biol. Chem.* *272*, 8215–8221.
- Meister, M., Lowe, G., and Berg, H.C. (1987). The proton flux through the bacterial flagellar motor. *Cell* *49*, 643–650.
- Milgrom, Y.M., Murataliev, M.B., and Boyer, P.D. (1998). Bi-site activation occurs with the native and nucleotide-depleted mitochondrial  $F_1$ -ATPase. *Biochem. J.* *330*, 1037–1043.
- Mitchell, P. (1961). Coupling of phosphorylation to electron and hydrogen transfer by a chemi-osmotic type of mechanism. *Nature* *191*, 144–148.
- Muneyuki, E., and Hirata, H. (1988). Kinetic analysis of proton translocation catalyzed by  $F_0F_1$ -ATPase. *FEBS Lett.* *234*, 455–458.
- Muneyuki, E., Kagawa, Y., and Hirata, H. (1989). Steady state kinetics of proton translocation catalyzed by thermophilic  $F_0F_1$ -ATPase reconstituted in planar bilayer membranes. *J. Biol. Chem.* *264*, 6092–6096.
- Muneyuki, E., Odaka, M., and Yoshida, M. (1997). A single mutation at the catalytic site of  $TF_1$ - $\alpha_3\beta_3\gamma$  complex switches the kinetics of ATP hydrolysis from negative to positive cooperativity. *FEBS Lett.* *413*, 55–59.
- Noji, H., Yasuda, R., Yoshida, M., and Kinosita, K., Jr. (1997). Direct observation of the rotation of  $F_1$ -ATPase. *Nature* *386*, 299–302.
- Oosawa, F., and Hayashi, S. (1986). The loose coupling mechanism in molecular machines of living cells. *Adv. Biophys.* *22*, 151–183.
- Sabbert, D., Engelbrecht, S., and Junge, W. (1996). Intersubunit rotation in active  $F_1$ -ATPase. *Nature* *381*, 623–625.
- Sase, I., Miyata, H., Corrie, J.E.T., Craik, J.S., and Kinosita, K., Jr. (1995). Real time imaging of single fluorophores on moving actin with an epifluorescence microscope. *Biophys. J.* *69*, 323–328.
- Sase, I., Miyata, H., Ishiwata, S., and Kinosita, K., Jr. (1997). Axial rotation of sliding actin filaments revealed by single-fluorophore imaging. *Proc. Natl. Acad. Sci. USA* *94*, 5646–5650.
- Soud, A.-K., and Penefsky, H.S. (1995). Energetics of ATP dissociation from the mitochondrial ATPase during oxidative phosphorylation. *J. Biol. Chem.* *270*, 9074–9082.
- Stryer, L. (1995). *Biochemistry*, Fourth Edition (New York: Freeman), pp. 443–462.
- Xiao, R., and Penefsky, H.S. (1994). Unisite catalysis and the  $\delta$  subunit of  $F_1$ -ATPase in *Escherichia coli*. *J. Biol. Chem.* *269*, 19232–19237.
- Yasuda, R., Noji, H., Kinosita, K., Jr., Motojima, F., and Yoshida, M. (1997). Rotation of the  $\gamma$  subunit in  $F_1$ -ATPase: evidence that ATP synthase is a rotary motor enzyme. *J. Bioenerg. Biomembr.* *29*, 207–209.
- Zhou, Y., Duncan, T.M., Bulygin, V.V., Hutcheon, M.L., and Cross, R.L. (1996). ATP hydrolysis by membrane-bound *Escherichia coli*  $F_0F_1$  causes rotation of the  $\gamma$  subunit relative to the  $\beta$  subunits. *Biochim. Biophys. Acta* *1275*, 96–100.